

Mapping of coherent and decohering nuclear wave-packet dynamics in D_2^+ with ultrashort laser pulses

Bernold Feuerstein and Uwe Thumm

Department of Physics, Kansas State University, Manhattan, Kansas 66506, USA

(Received 11 November 2002; published 26 June 2003)

Fast ionization of D_2 leads to the coherent population of many vibrational states of D_2^+ . Usually, only the squared absolute values of the vibrational state amplitudes, known as Franck-Condon factors, are observed since insufficient experimental time resolution averages out all coherence effects. We propose a Coulomb explosion imaging method to visualize the coherent motion of bound wave packets using ultrashort (5 fs), intense pump-probe laser pulses. With this type of experiment decoherence times in the fs to ps range may become directly observable and provide essential information for coherent control.

DOI: 10.1103/PhysRevA.67.063408

PACS number(s): 33.80.Rv, 33.90.+h, 34.50.Gb, 03.65.Yz

The H_2^+ (D_2^+) molecular ion is of fundamental interest in atomic and molecular physics. Together with its atomic counterparts (H^- and He), this simplest molecule represents a bound three-body Coulomb system. In contrast to the atomic systems, the molecule exhibits (if we neglect rotation) two timescales, the fast electronic motion (as scale) and the vibrational motion of the nuclei (fs scale). The interaction of these smallest molecules with strong fs laser pulses is of particular interest, since the pulse duration is comparable to the vibrational period [14 fs for H_2^+ ($\nu=0$)]. For homonuclear systems, the nuclei do not couple directly to the laser field due to the lack of a permanent electric dipole moment. Thus, the dynamics in the laser field is dominated by the interaction of the electron with the field, which acts only indirectly back on the nuclei via non-Born-Oppenheimer couplings.

Numerous theoretical investigations on H_2^+ in strong laser fields have been done so far emphasizing the influence of the two-center nature of the electronic potential on strong-field ionization [1–10]. Here, the laser-induced coupling of the lowest electronic states leads to an oscillating localization of the electron near one of the nuclei. This gives rise to dissociation of the molecule and to “charge resonance enhanced ionization” at intermediate internuclear distances R between 5 and 10 a.u. [2,4]. Experimentally, the situation is more challenging, since mostly neutral H_2 (D_2) targets are available [1,11–18], such that the production and fragmentation of the molecular ion occurring in the same laser pulse are difficult to separate. It was shown that for 50 fs pulses, saturation of H_2^+ is never reached at any intensity [14]. Moreover, a recent kinematically complete study for all ionization and fragmentation channels of H_2 revealed the breakdown of the simple two-step model of production and fragmentation of H_2^+ [18], i.e., the correlation of the two electrons has to be taken into account. To overcome this problem, attempts have been made to get either more detailed information on the time evolution of the molecule during the laser pulse [14,15] or to use a molecular ion beam as the target [19].

Due to advances in ultrashort pulse technology, pulse durations down to 5 fs are now available [20], and Coulomb explosion (CE) imaging of bound and moving nuclear wave

packets [21] should become feasible even for light molecules such as H_2 . Further, ultrashort pulses enable pump-probe experiments that separate the production and fragmentation of the molecular ion. The time-resolved observation of the nuclear motion will reveal coherence effects, which we describe within the density matrix formalism, starting with a coherent superposition of vibrational eigenstates φ_k ,

$$\Phi(R, t) = \sum_k a_k \exp(-i\omega_k t) \varphi_k(R). \quad (1)$$

The probability density of this state can be expressed in terms of the time-dependent density matrix $\rho_{km} = a_k a_m^* \exp(-i\omega_{km} t)$ with $\omega_{km} = \omega_k - \omega_m$,

$$|\Phi(R, t)|^2 = \sum_k \rho_{kk} |\varphi_k|^2 + \sum_{k \neq m} \rho_{km}(t) \varphi_k \varphi_m^*. \quad (2)$$

Averaging over a time T results in

$$\overline{|\Phi(R, T)|^2} = \sum_k \rho_{kk} |\varphi_k|^2 - \sum_{k \neq m} a_k a_m^* \varphi_k \varphi_m^* \frac{\exp(-i\omega_{km} T) - 1}{i\omega_{km} T}. \quad (3)$$

The first sum, containing only diagonal elements of the density matrix, corresponds to an incoherent mixture of eigenstates. The coherence—expressed by the off-diagonal elements in the second term—vanishes for a sufficiently large averaging time $T \gg \omega_{km}^{-1}$. Then, the time average is equivalent to an ensemble average. In two recent experiments [19], the H_2^+ ions have been prepared in an ion source. The uncertainty in the time delay between production of the molecular ions and the interaction with the laser pulse is of the order of μs . Thus, coherence effects on the fs timescale are averaged out according to Eq. (3). Similarly, environment-induced decoherence [22] should yield a stationary probability distribution after a sufficiently long time T . Information about decoherence times is of great importance for the coherent control of quantum systems.

The aim of this paper is twofold. First, we model the fragmentation of D_2^+ out of the vibrational ground state (ν

$=0$) in a two-pulse laser field. We consider D_2^+ rather than H_2^+ in order to take advantage of the slower nuclear motion. Our numerical results will be compared with a recent experiment [15]. Second, we propose a pump-probe experiment for the neutral D_2 molecule in order to image the coherent nuclear wave packet dynamics. We use atomic units, except where otherwise indicated.

The molecular ion is described in a reduced-dimensionality collinear model in terms of the electronic coordinate z relative to the center of mass of the nuclei and the internuclear distance R . The model-inherent alignment of the molecule along the polarization axis of the laser electric field $F(t)$ is not a serious problem since in a kinematically complete experiment fragmentation along this axis can be selected. Further, for linearly polarized nonrelativistic laser fields considered here, only the coordinates parallel to the electric field vector play an important role. Our model includes the (non-Born–Oppenheimer) coupling between the electronic and nuclear motion. The Hamiltonian is given by

$$H = T_n + 1/R + T_e + V_{en} - zF(t), \quad (4a)$$

$$V_{en} = -1/\sqrt{z_-^2 + a(R)^2} - 1/\sqrt{z_+^2 + a(R)^2}, \quad (4b)$$

with $z_{\pm} = z \pm R/2$. T_n and T_e are the kinetic energies for the nuclei and the electron, respectively. Softcore Coulomb potentials [23] are used for the electron-nucleus interaction with an R -dependent softening function $a(R)$, which is adjusted to exactly reproduce the electronic ground-state potential curve [24]. We solve the time-dependent Schrödinger equation numerically on a grid using the Crank-Nicholson split-operator method [25]. The grid extends from 0.05 to 30 in R with a spacing of 0.05 and from -45 to 45 in z with a spacing of 0.2. Absorbing regions using an optical potential are introduced over the last 200 (in R) and 100 (in z) grid points in order to prevent a reflection of the outgoing wave packets by the border of the grid. The number of time steps per optical cycle is 1100. Each time step the norm of the total wave function within $0.05 \leq R \leq 20$, $-25 \leq z \leq 25$ is calculated. The outgoing flux through the borders of this inner part of the grid can be used to obtain differential and integrated data on the fragmentation process. The dissociation yield into the $D^+ + D$ fragmentation channel is given by the time-integrated flux in the R direction at $R=20$. Removal of the electron leads to CE (into $D^+ + D^+ + e^-$), the yield of which is given by the time-integrated electronic flux in the z direction at $z = \pm 25$. From the time-dependent phase of the outgoing nuclear wave packets at $R=20$, we derive the nuclear momentum distribution for dissociation using the “virtual detector” method [26]. The CE spectra are obtained by first computing the ionization rate as the outgoing electron flux at a given position R . During the (fast) ionization of the electron we treat the (slow) nuclei as “frozen.” For each position R , the Coulomb energy $1/R$ is released. In order to take the initial (dissociative) velocity of the nuclei into account, we add the Coulomb energy and the initial kinetic energy $E_{\text{init}}(R)$ of the nuclei at the ionization time and obtain the final kinetic energy of the fragments,

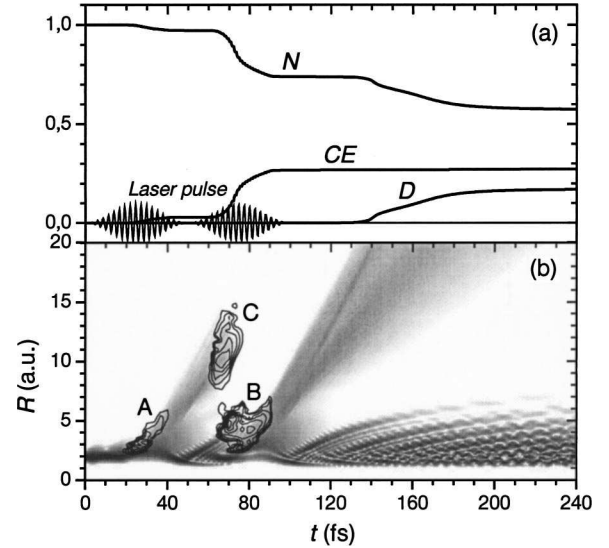


FIG. 1. (a) Time-dependent norm (N) and probabilities for Coulomb explosion (CE) and dissociation (D) of D_2^+ ($\nu=0$) in a two-pulse laser field (25 fs, 0.3 PW/cm^2 , 50 fs delay). (b) Corresponding probability density $|\Phi(R,t)|^2$ (logarithmic gray scale) and ionization rates (contour lines).

$$E_{\text{kin}} = 1/R + E_{\text{init}}(R). \quad (5)$$

Figure 1(a) shows the time-dependent norm N and the yield for dissociation D and CE for D_2^+ ($\nu=0$) and two 25 fs laser pulses of 0.3 PW/cm^2 intensity and a delay $\tau = 50$ fs. The time evolution of the probability density $P(R,t) = |\Phi(R,t)|^2$ is shown in Fig. 1(b) with contour lines indicating the electronic ionization rate. Three different ionization regions can be distinguished: ionization from bound vibrational states during the first (A) and second (B) laser pulse and delayed ionization of the dissociating wave packet (C). Figure 2 shows the corresponding total fragment kinetic energy spectra for delays of 30, 50, and 70 fs. The low-energy part of the spectrum is due to dissociation via the Floquet one- and two-photon channels [11]. The CE spectra map ionization events in regions A, B, and C. The broad peak A (5–13 eV) shows no delay dependence. Its large width complies with the ionization rates in Fig. 1(b) and Eq. (5). Besides ionization, the first pulse induces dissociation and excitation into a coherent superposition of bound vibrational states. During the second pulse we find ionization of the bound part (peak B) and delayed ionization of the continuum part of the wave packet (peak C). Peak B is delay dependent due to the coherent motion of the bound wave packet. Peak C moves towards lower kinetic energies with increasing τ and finally merges with the dissociation peaks for large τ , since the energy due to CE becomes small at large R . This kind of imaging has been recently reported for D_2^+ [15]. The experiment used a D_2 target and 80 fs laser pulses and revealed a delay-dependent peak in the kinetic energy spectra (Fig. 2 of [15]), which shows the same delay dependence as peak C in our model.

The behavior of peak B reflects the coherent motion of the bound wave packet and suggests a pump-probe study of the

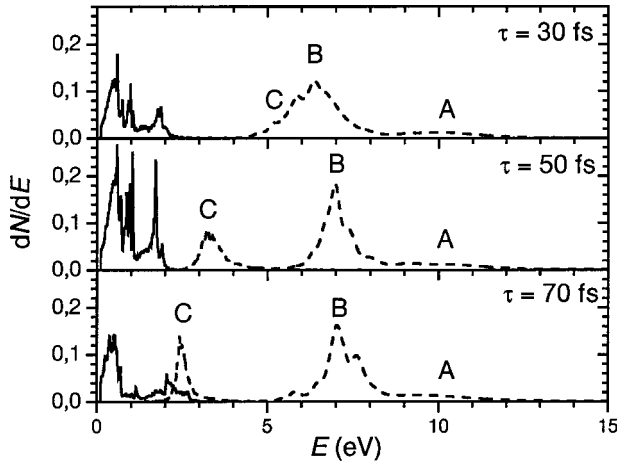


FIG. 2. Kinetic energy spectra for dissociation (solid lines) and Coulomb explosion (dashed lines) of D_2^+ ($\nu=0$) in a two-pulse laser field (25 fs, 0.3 PW/cm^2) with variable delay τ . The features A–C correspond to the ionization regions in Fig. 1(b).

neutral molecule using ultrashort (<10 fs) laser pulses. For neutral targets and pulse durations >50 fs, production and fragmentation of D_2^+ cannot be easily separated. On the other hand, molecular ion beams cannot reveal coherence since the ions have to be treated as a statistical ensemble. We therefore propose to first (almost) completely ionize D_2 with an ultrashort (5 fs), intense (1 PW/cm^2) pulse within less than 2 fs near the pulse maximum [21]. The ionization time is short compared to the classical oscillation time for the D_2 ($\nu=0$) state of 20 fs. Hence, the ionization can be treated as a vertical (Franck-Condon) transition where the D_2 ($\nu=0$) initial wave function is projected onto the D_2^+ potential curve. We start the calculation in the center of the first pulse. Since the assumed intensity of the 5 fs pump pulse is high enough to saturate the D_2^+ production, the ionization probability does not depend on R .

Our calculation shows D_2^+ ions that are prepared at the center of a 1-PW/cm^2 5 fs pulse and survive with a high probability the remaining half pulse. Thus, these pulse parameters are suitable for experimental studies and avoid double ionization contributions from the first pulse. The dissociation (ionization) yield due to the half pulse is 2% (1.7%). For H_2^+ , we find 11% (4%). The higher stability of D_2^+ originates in the slower nuclear motion. Figure 3(a) illustrates the coherent nuclear wave packet dynamics of D_2^+ following the vertical transition from D_2 ($\nu=0$). The expectation value $\langle R \rangle$ starts at the equilibrium distance of D_2 ($\nu=0$), $R_0=1.4$. After a few oscillations, the anharmonicity of the potential curve, i.e., the nonequal spacing of the vibrational levels, leads to the “collapse” of the wave packet. For $t \approx 580$ fs, we find a partial revival of the wave packet. A measure for the collapse and revival is the autocorrelation function $|\langle \Phi(t=0) | \Phi(t) \rangle|^2$ [Fig. 3(b)].

A second laser pulse, strong enough to ensure complete ionization of D_2^+ , can probe the time evolution of the wave packet. In this case CE allows a mapping of $P(R, t) = |\Phi(R, t)|^2$. The measured kinetic energy distribution

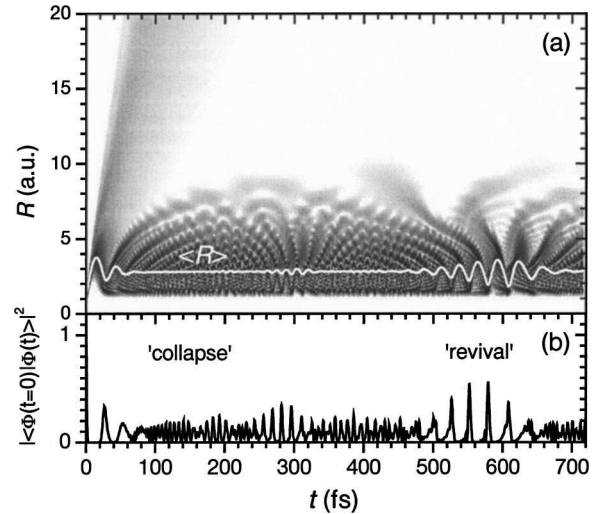


FIG. 3. Coherent motion of the D_2^+ nuclear wave packet following ionization of D_2 ($\nu=0$) in a 5-fs, 1-PW/cm^2 laser pulse. (a) Probability density $|\Phi(R, t)|^2$ (logarithmic gray scale) and expectation value $\langle R \rangle$. (b) Autocorrelation function.

$KE(E, \tau)$ for a given τ of the probe pulse is then transformed to the reconstructed probability density

$$P'(R, \tau) = KE(E_C(R), \tau) / R^2. \quad (6)$$

This transformation neglects the kinetic energy of the nuclear motion at the ionization time τ [21]. In general, the accuracy of this imaging method is limited by (1) the finite ionization time during the probe pulse (<2 fs), (2) the initial average

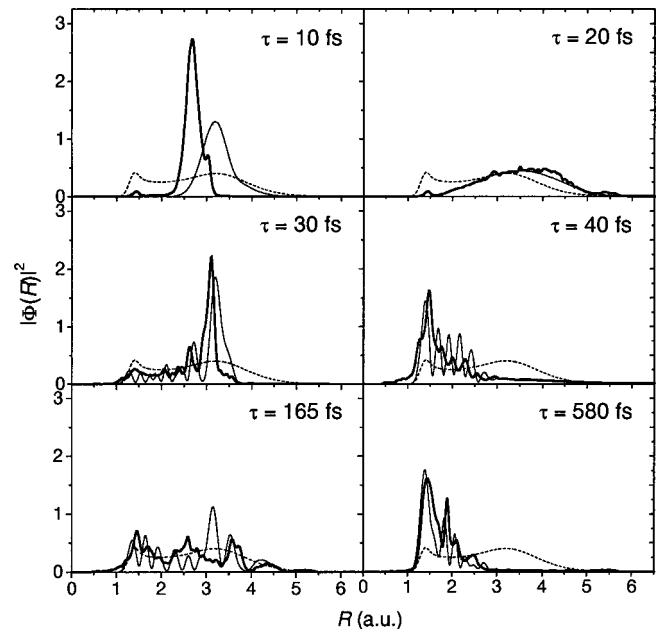


FIG. 4. Snapshots of the coherent nuclear motion in D_2^+ following ionization of D_2 ($\nu=0$) in a 5-fs, 1-PW/cm^2 laser pulse for various delays τ of the probe pulse. Thick solid line: reconstructed probability density $P'(R)$. Thin solid line: original density $|\Phi(R, \tau)|^2$. The incoherent Franck-Condon distribution is given by the dashed lines.

(group) velocity of the wave packet, and (3) the *inherent* momentum spread due to the uncertainty principle. (1) and (3) are similar to the photographic blurring effect for a finite exposure time. (2) leads to a shift of $P'(R, \tau)$ towards smaller R (i.e., larger kinetic energy release). In contrast to (1), the effect (3) remains, even in the limit of an instant ionization. An upper limit for the influence of (3) is obtained from the initial width of the wave packet, $\Delta R_{\text{WP}} \geq 0.2$, which leads to a finite image resolution of $\Delta R_{\text{image}} \leq 0.1$.

Figure 4 shows $P'(R, \tau)$ compared with the original probability density $P(R, \tau) = |\Phi(R, \tau)|^2$ for selected τ values. The intensity of the 5 fs probe pulse is 2 PW/cm². For $\tau = 10$ fs, the shift of the reconstructed distribution towards smaller R due to the kinetic energy of the wave packet becomes obvious. This effect is less important close to the turning point of the oscillating wave packet at $\tau = 20$ fs. The partial revival at $\tau = 580$ fs shows the wave packet with its maximum close to the equilibrium distance of D₂. In the region of the “collapse” of the wave packet, the interference structures are partially shifted and partially averaged out due to the effects (1) and (3). However, if coherence is preserved, the time-dependent nuclear motion should be observable in CE imaging. Further, if decoherence occurs due to coupling to other degrees of freedom (e.g., rotation) or to a thermal background, it should manifest itself in a breakdown of the

time dependence. Thus, after a “decoherence time” the CE spectra become independent of τ , and the reconstructed wave packet merges into an incoherent Franck-Condon distribution. This offers, in principle, a direct measure of decoherence times of a quantum system. Since the direct coupling of the homonuclear D₂⁺ to the thermal radiation is very weak due to the lack of a permanent electric dipole moment, an experimental study with HD⁺ could demonstrate the influence of coupling strengths on the decoherence time.

In conclusion, the development of ultrashort (5 fs), intense laser pulses enables pump-probe studies of the nuclear wave packet dynamics even for light molecular systems such as H₂⁺ or D₂⁺. Dissociating wave packets as well as the coherent motion of bound states can be probed on a fs time scale. This method should enable the direct measurement of decoherence times on a fs to ps time scale and, thus, provide important information for the coherent control of quantum systems.

This work was supported by the Division of Chemical Sciences, Office of Basic Energy Sciences, Office of Energy Research, U.S. DOE, and NSF Grant No. PHY-0071035. B.F. acknowledges a research scholarship from the DFG (Germany).

-
- [1] A. Giusti-Suzor, F. H. Mies, L. F. DiMauro, E. Charron, and Y. Yang, *J. Phys. B* **28**, 309 (1995).
- [2] T. Seidemann, M. Yu Ivanov, and P. B. Corkum, *Phys. Rev. Lett.* **75**, 2819 (1995); T. Zuo and A. D. Bandrauk, *Phys. Rev. A* **52**, R2511 (1995).
- [3] K. C. Kulander, F. H. Mies, and K. J. Schafer, *Phys. Rev. A* **53**, 2562 (1996).
- [4] S. Chelkowski, A. Conjusteau, T. Zou, and A. D. Bandrauk, *Phys. Rev. A* **54**, 3525 (1996).
- [5] M. Plummer and J. F. McCann, *J. Phys. B* **29**, 4625 (1996).
- [6] T. D. G. Walsh *et al.*, *Phys. Rev. A* **58**, 3922 (1998).
- [7] I. Kawata, H. Kono, and Y. Fujimura, *J. Chem. Phys.* **110**, 11152 (1999).
- [8] D. Dundas, J. F. McCann, J. S. Parker, and K. T. Taylor, *J. Phys. B* **33**, 3261 (2000).
- [9] Y. Duan, W.-K. Liu, and J.-M. Yuan, *Phys. Rev. A* **61**, 053403 (2000).
- [10] M. E. Sukharev and V. P. Krainov, *Phys. Rev. A* **62**, 033404 (2000).
- [11] G. N. Gibson, M. Li, C. Guo, and J. Neira, *Phys. Rev. Lett.* **79**, 2022 (1997).
- [12] T. D. G. Walsh, F. A. Ilkov, and S. L. Chin, *J. Phys. B* **30**, 2167 (1997).
- [13] L. J. Frasinski *et al.*, *Phys. Rev. Lett.* **83**, 3625 (1999).
- [14] J. H. Posthumus *et al.*, *J. Phys. B* **32**, L93 (1999).
- [15] C. Trump, H. Rottke, and W. Sandner, *Phys. Rev. A* **59**, 2858 (1999).
- [16] C. Trump, H. Rottke, and W. Sandner, *Phys. Rev. A* **60**, 3924 (1999); C. Trump *et al.*, *ibid.* **62**, 063402 (2000).
- [17] A. Staudte *et al.*, *Phys. Rev. A* **65**, 020703 (2002).
- [18] H. Rottke *et al.*, *Phys. Rev. Lett.* **89**, 013001 (2002).
- [19] K. Sändig, H. Figger, and T. W. Hänsch, *Phys. Rev. Lett.* **85**, 4876 (2000); I. D. Williams *et al.*, *J. Phys. B* **33**, 2743 (2000).
- [20] T. Brabec and F. Krausz, *Rev. Mod. Phys.* **72**, 545 (2000); Q. Apolonski *et al.*, *Phys. Rev. Lett.* **85**, 470 (2000); C. Spielmann *et al.*, *Science* (Washington, DC, U.S.) **278**, 661 (1997).
- [21] S. Chelkowski, P. B. Corkum, and A. D. Bandrauk, *Phys. Rev. Lett.* **82**, 3416 (1999); S. Chelkowski and A. D. Bandrauk, *Phys. Rev. A* **65**, 023403 (2002).
- [22] F. B. J. Buchkremer, R. Dumke, H. Levsen, G. Birkl, and W. Ertmer, *Phys. Rev. Lett.* **85**, 3121 (2000); S. Wallentowitz, I. A. Walmsley, L. J. Waxer, and Th. Richter, *J. Phys. B* **35**, 1967 (2002).
- [23] Q. Su and J. H. Eberly, *Phys. Rev. A* **44**, 5997 (1991).
- [24] B. Feuerstein and U. Thumm, *Phys. Rev. A* **67**, 043405 (2003).
- [25] W. H. Press, S. A. Teukolsky, W. T. Vetterling, and B. F. Flannery, *Numerical Recipes* (Cambridge University Press, Cambridge, 1992), p. 842.
- [26] B. Feuerstein and U. Thumm, *J. Phys. B* **36**, 707 (2003).